Reduced graphene oxide decorated with ZnO microrods for efficient electromagnetic wave absorption performance

Yi Liu[1] · Xiaomei Du[1] · Congya Wu[1] · Yanan Liu[1] · Yaqing Liu[1] · Guizhe Zhao[1]

Abstract

A composite RGO/ZnO-mrs, which is reduced graphene oxide (RGO) decorated with ZnO microrods (ZnO-mrs), with excellent electromagnetic wave absorbing performance was prepared by a simple mechanical mixing and direct freeze-drying method. The load of ZnO-mrs in this composite is controlled effectively by changing mass ratio of raw materials $Zn(Ac)_2 \cdot 2H_2O$ and graphene oxide (GO), then the balance between dielectric loss ability to electromagnetic wave and impedance matching with free space of the absorbing composite RGO/ZnO-mrs prepared can be obtained, and then its high-performance electromagnetic wave absorption ability. When mass ratio of GO to $Zn(Ac)_2 \cdot 2H_2O$ is 1:3, composite RGO/ZnO-mrs filled with only 15 wt% exhibits the most significant electromagnetic wave absorption properties, its minimum reflection loss (RL_{min}) value of -38.5 dB is obtained at 15.4 GHz and effective absorption bandwidth (EAB) is up to 5.4 GHz (12.6–18 GHz) with a thickness of 2 mm only. The basic electromagnetic wave absorption mechanism of this composite is discussed systematically. All results demonstrate that composite RGO/ZnO-mrs in this study is very promising as a broadband absorption, light weight, especially with a simple and expandable preparing process electromagnetic wave absorber.

1 Introduction

In recent years, with the explosive growth of electronic equipment in industrial, commercial and military fields, electromagnetic wave (EMW) pollution has been attracting extensive attention, so EMW absorbing materials have been developing rapidly [1, 2]. Excellent EMW absorption materials must have properties such as light weight, high stability, strong absorption and wide absorption band [3, 4]. As a representative of EMW absorbing materials, RGO is developing rapidly due to its unique two-dimensional structure and excellent performances, such as low density, high specific surface area, high conductivity and outstanding dielectric loss [5–7]. Through appropriate preparation process, pure RGO can display certain EMW absorption performance [8–10]. Development of functional RGO modified with

magnetic materials also represents an important progress in improving its electromagnetic absorption properties, such as RGO-Fe$_3$O$_4$ [11], RGO-CIP@Fe$_3$O$_4$ [12], RGO-Co$_3$O$_4$ [13], RGO-ZnO @Fe$_3$O$_4$ [14] and RGO/Ni [15], which can not only improve impedance matching of RGO with free space, but also increase its EMW absorption ability.

ZnO, as an important semiconductor with wide band gap, has been widely studied in many fields, such as solar cells, sensors, optics and optoelectronics. Recently, it was proved to be an ideal candidate for microwave absorption applications due to its semiconducting property and easy to realize large-scale synthesis. Moreover, compared with the traditional magnetic loss materials, adding dielectric loss materials can broaden absorption band and reduce the loading dosage required in the matrix, which is convenient for practical application [16, 17]. And because of the unique properties of RGO and ZnO and their synergistic effects, many applications of their composites have been investigated. Recently, their EMW absorption properties have also been reported. Song et al. combined RGO foam with ZnO nanowires grown in situ, and their dielectric and microwave absorption properties were studied too [18]. Wei et al. synthesized RGO decorated with well-dispersed ZnO nanocrystals using in situ growth strategy and obtained an EMW absorption material with light weights[19]. Yang et al. developed 3D graphene

✉ Yaqing Liu
lyq@nuc.edu.cn

✉ Guizhe Zhao
zgz@nuc.edu.cn

[1] Shanxi Province Key Laboratory of Functional Nanocomposites, College of Materials Science and Engineering, North University of China, Taiyuan 030051, People's Republic of China

and shuttle-shaped ZnO nanoparticles prepared in solution phase by a novel and simple two-step method, which showed EMW absorption properties enhanced [20]. It is found that all ZnO with different morphologies can possess outstanding absorbing properties. According to the definition of the electric dipole moment, it can be concluded that one-dimensional ZnO-mrs has higher electric dipole moment than that of ZnO with other shapes, such as sphere and star, which results in stronger dipole polarization of one-dimensional ZnO-mrs. In addition, the free charges tend to gather at the grain boundaries, phase boundaries, lattice distortions and defects; the more complex the interfaces, the more charge accumulations, and the stronger the interface polarization. So the interfacial polarization intensity of one-dimensional ZnO-mrs is stronger than that of spherical ZnO. On the other hand, the one-dimensional ZnO-mrs has better stability than that of star-shaped ZnO. Therefore, its composite has a higher absorbing stability to EMW and a great prospect in application.

Then, in this work, chemically reduced GO compounded with ZnO-mrs was prepared by a very simple way, its dielectric constant can be adjusted easily by controlling ZnO-mrs loads, thus resulting in the balance between its dielectric loss to EMW and impedance matching with free space. Therefore, composite RGO/ZnO-mrs in this study shows excellent EMW absorption properties, and has great potential in the development of light weight and high efficiency, especially with a simple and expandable preparing process electromagnetic wave absorber.

2 Experimental sections

2.1 Materials

The commercial graphene oxide suspension (GO) (1 mg/mL) was purchased from Tangshan Jianhua Technology Co., Ltd, China. Zinc acetate dihydrate ($Zn(Ac)_2 \cdot 2H_2O$) and Hydrazine hydrate (40% by volume) were all obtained from Tianjin Beichen Founder Reagent Factory, China. Polyvinyl pyrrolidone (PVP) (K30) was got from Tianjin Damao Chemical Reagent Factory, China. All chemicals in this study were of analytical grade and used directly without further purification.

2.2 Synthesis of ZnO-mrs

ZnO-mrs crystals were synthesized via chemical bath deposition method. A typical synthesis procedure was as follows: 1.5 g of $Zn(Ac)_2 \cdot 2H_2O$ and 1.5 g of PVP were dissolved in 80 mL of deionized water with stirring at room temperature, reacted for 6 h at 80 °C to stationary state. ZnO-mrs crystals

obtained were washed with deionized water and ethanol several times.

2.3 Preparation of RGO/ZnO-mrs

The above-prepared ZnO-mrs crystals were added into 50 mL of GO aqueous solution and agitated ultrasonically for 60 min, and then hydrazine hydrate was dropped into the mixed solution according to the mass ratio of 1:57 to GO and stirred for 3 h at 95 °C. The resulting precipitates were separated from the supernatant by filtration, and then washed with distilled water several times to remove the redundant ions. After freeze-drying, the target product RGO/ZnO-mrs was finally obtained. The same method was used to prepare RGO without adding ZnO-mrs. Composites, prepared with different molar ratios of GO and $Zn(Ac)_2 \cdot 2H_2O$, specifically 1:0.005, 1:0.008 and 1:0.01, were designated as RGO/ZnO-mrs-1, RGO/ZnO-mrs-2 and RGO/ZnO-mrs-3, respectively.

2.4 Characterizations

Morphology of materials was examined by a scanning electron microscopy (SEM, Hitachi SU8010) and a transmission electron microscopy (TEM, JEOL, 2100F). The aspect ratio of ZnO-mrs was measured by Image J software. Crystal phase of samples was identified by an X-ray diffraction (XRD; Haoyuan, DX2700B) using Cu Ka ($\lambda = 1.5406$ Å) radiation. To confirm the functional groups on sample surfaces, X-ray photoelectron spectrum was measured by an X-ray photoelectron spectrometer (XPS, ESCALAB210). Conductivity of materials was measured by a four-probe tester (RTS-9). Thermogravimetric analysis was carried out using a thermal gravimetric analyzer (TGA, Q50) in the temperature range of 40–800 °C at the heating rate of 10 °C min^{-1} in the air flow. The permittivity and permeability of materials were obtained by an Agilent N5232A vector network analyzer in the frequency range of 2–18 GHz and their microwave absorption performances were calculated according to the transmission line theory. 15 wt% RGO/ZnO-mrs mixed evenly with the molten paraffin was pressed into a standard ring with an outer diameter of 7 mm, an inner diameter of 3.04 mm and a thickness of 2.5 mm.

3 Results and discussion

3.1 Microstructure characterization

Figure 1a shows the XRD patterns of RGO, ZnO-mrs and RGO/ZnO-mrs-2. The broad diffraction peak around $2\theta = 22°$ observed should correspond to the (002) crystal surface of RGO, indicating that GO is reduced to RGO [21].
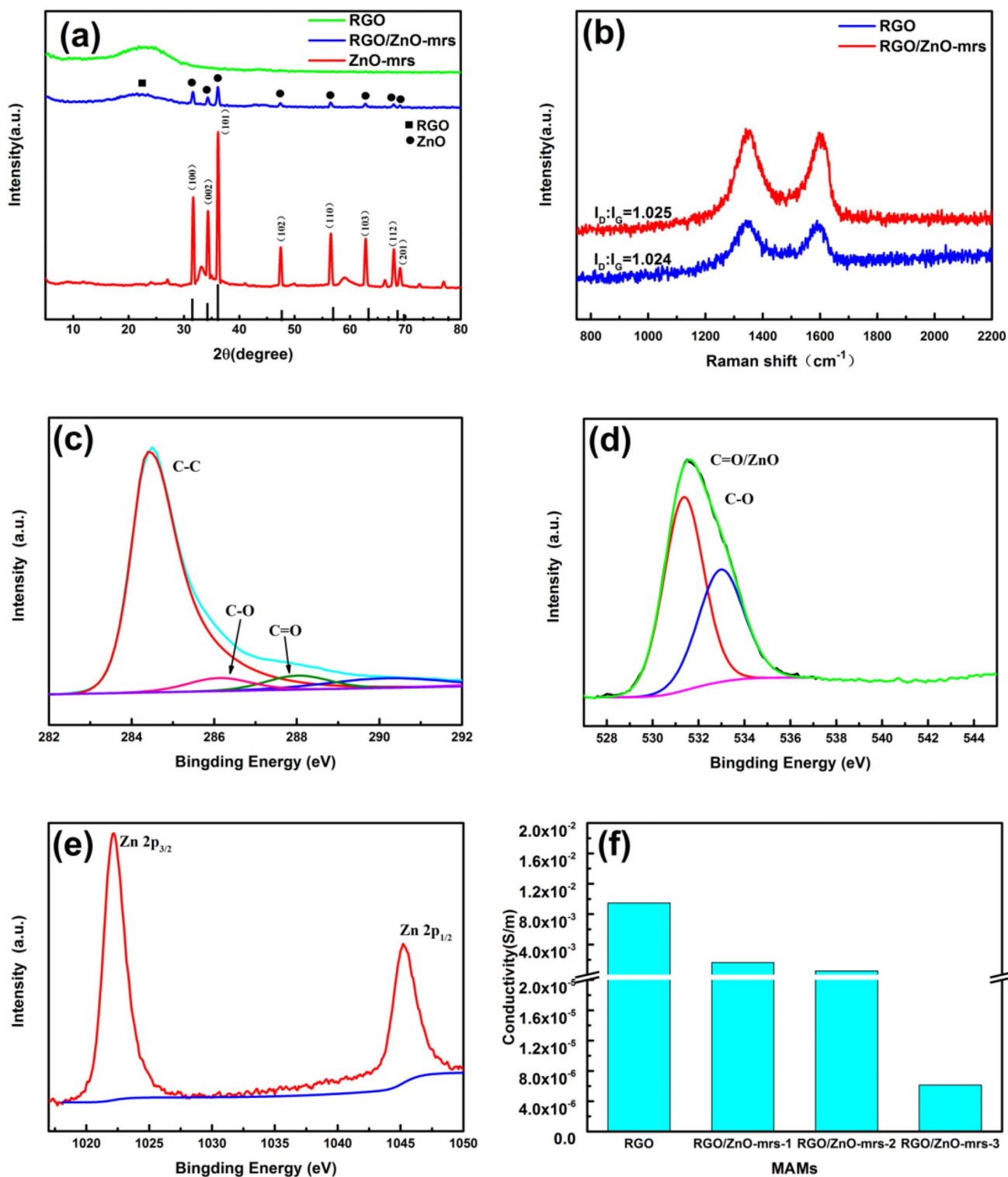
Fig. 1 XRD spectra (**a**) of RGO, ZnO-mrs and RGO/ZnO-mrs-2; Raman spectra (**b**) of RGO and RGO/ZnO-mrs-2; XPS spectra of (**c**) C 1s, (**d**) O 1s and (**e**) Zn 2p of RGO/ZnO-mrs-2; (**f**) electrical conductivities of RGO and RGO/ZnO-mrs composites

The diffraction peaks of ZnO can be observed at $2\theta = 31.5, 34.1, 36.0, 47.3, 56.3, 62.6, 67.6$ and $68.6°$, corresponding to its (100), (002), (101), (102), (110), (103), (112) and (201) planes, respectively, which are consistent with the standard spectrum of ZnO with hexagonal wurtzite crystal structure [22]. No other peaks are observed, indicating

ZnO-mrs was prepared with high crystal quality. There are only peaks of RGO and ZnO-mrs in RGO/ZnO-mrs-2, indicating that there are no other impurities in RGO/ZnO-mrs-2 prepared. Figure 1b shows Raman spectra of RGO and RGO/ZnO-mrs-2. Two typical Raman peaks at 1345 cm^{-1} and 1580 cm^{-1} are observed, corresponding to D-band and G-band, respectively. G peak represents the Raman-active E_{2g} mode, characterizing the sp^2 hybridized C–C bond in RGO, while D peak is caused by the in-plane vibration of sp^3 carbon atom, reflecting the disorder degree of the crystal structure, which is related to the defects and dangling bonds [23]. Therefore, the intensity ratio I_D/I_G is commonly used as the index of lattice defect density and reduction degree of carbon materials. The more the lattice defects exist, the stronger the reduction degree is, and the higher intensity ratio of I_D/I_G is obtained [24]. In this work, with the addition of ZnO-mrs, the I_D/I_G values increase from 1.024 of RGO to 1.025 of RGO/ZnO-mrs-2 without significant changes, indicating that ZnO-mrs has no effects on the reduction process of RGO. Figure 1c shows the XPS spectra of C 1s of RGO/ZnO-mrs-2, which exhibits three fitting peaks at binding energies of 284.4, 286 and 288.5 eV, attributing to the C–C, C–O and C=O groups in aromatic rings, respectively. The intensities of the characteristic peaks of C–O and C=O are weak, suggesting a remarkable reduction of GO [25]. Figure 1d reveals XPS spectra of O 1s of RGO/ZnO-mrs-2, which can be divided into two peaks, and the characteristic peak at 531.5 eV is related to the original lattice oxygen species of ZnO. In Fig. 1e, peaks in the spectra of Zn 2p are observed at 1044.3 and 1021.3 eV, which originate from Zn 2p$_{1/2}$ and Zn 2p$_{3/2}$ [20]. Figure 1f displays the conductivity of RGO and RGO/ZnO-mrs; it can be seen that the conductivity of RGO is the highest, reaching 9.46×10^{-3} S/m, while the conductivity of RGO/ZnO-mrs decreases obviously with the addition of semiconducting material ZnO-mrs, which helps to reduce the dielectric constant of the composites, then reduce its reflection to EMW, improve its impedance matching with free space and facilitate the absorption to electromagnetic wave

To know the micro-morphologies of these materials, SEM and TEM tests were carried out, and the results are shown in Fig. 2. From Fig. 2a, the RGO sheets display a crumpled structure due to the deformation during the processes of exfoliation and restack. They are closely interconnected and stacked, forming an open network structure. As shown in Fig. 2b, the pure RGO sheets without loading ZnO have many folds which lead to their low transparency. From Fig. 2c, the prepared ZnO is regular rod-shaped with a length of about 3 μm. Figure 2d and e shows RGO/ZnO-mrs-2 with different magnifications; it can be seen that ZnO-mrs are dispersed on the surfaces of GO sheets and wrapped by these sheets; moreover, after loading ZnO, the RGO sheets become loose, showing that ZnO-mrs can effectively prevent

the agglomeration of GO sheets, which is also confirmed by the TEM test result in Fig. 2f. In addition, Fig. 2f also shows that the RGO sheets loaded with ZnO-mrs have fewer folds and higher transparency than those of pure RGO. Figure 2g shows that the average length of ZnO-mrs determined by dimension software is 2.97 μm, while Fig. 2h shows that its average short diameter is 1.79 μm, so the aspect ratio of ZnO-mrs is 1.65.

TG analysis results of RGO/ZnO-mrs with different ZnO-mrs loading amounts are shown in Fig. 3. These TG curves decrease slightly before 350 °C, which is due to the removal of residual oxygen-containing functional groups in RGO; after 400 °C, they drop sharply and remain stable after 600 °C, indicating the complete removal of RGO [18], for RGO can be completely burned in air, so the residues should be ZnO-mrs only. Based on the TG curves, the mass ratios of RGO to ZnO-mrs in composites prepared are 1:1.9, 1:3 and 1:4, corresponding to RGO/ZnO-mrs-1, RGO/ZnO-mrs-2 and RGO/ZnO-mrs-3, respectively.

3.2 Dielectric constant and microwave absorption performance

Microwave absorption properties of materials are closely related to their complex permittivity ($\varepsilon_r = \varepsilon' - j\varepsilon''$) and complex permeability ($\mu_r = \mu' - j\mu''$), their real parts ε' and μ' show the ability to store electric and magnetic energy, while their imaginary parts ε'' and μ'' represent the loss ability to electric and magnetic energy [26, 27]. Since there is no magnetic component in composites of this study and paraffin, values of μ' and μ'' of materials are all close to 1 and 0 respectively, as shown in Fig. 4c and d. In Fig. 1a, values of ε' and ε'' of both RGO and RGO/ZnO-mrs all present a similar downward trend with the increase of frequency, but the downward trend becomes less obvious with the increase of ZnO-mrs loads. RGO, RGO/ZnO-mrs-1 and RGO/ZnO-mrs-2 have significant fluctuations in range of 12–18 GHz. Values of ε'' of all samples exhibit a similar change trend. It can be seen from ε''–f curves that there are multiple resonance peaks in range of 8–18 GHz, and these resonance behaviors may be related to the interfaces between RGO/air, ZnO-mrs/air and RGO/ZnO-mrs [28, 29]. Moreover, ε'' values of RGO-/ZnO-mrs-1 decrease suddenly after 16 GHz, which should be related to the frequency-dependent dielectric dispersion in carbon-based composites [11]. Compared with that of neat RGO, values of ε' and ε'' of composites decrease significantly with the addition of ZnO-mrs; in addition, with the increase of the contents of ZnO-mrs, the ε' and ε'' of RGO/ZnO-mrs also decrease significantly, which should be due to the low conductivity of component ZnO-mrs resulting in low dielectric constant. Value of dielectric loss tangent ($\tan\delta_E = \varepsilon''/\varepsilon'$) is a physical quantity which characterizes the material's ability of dielectric loss
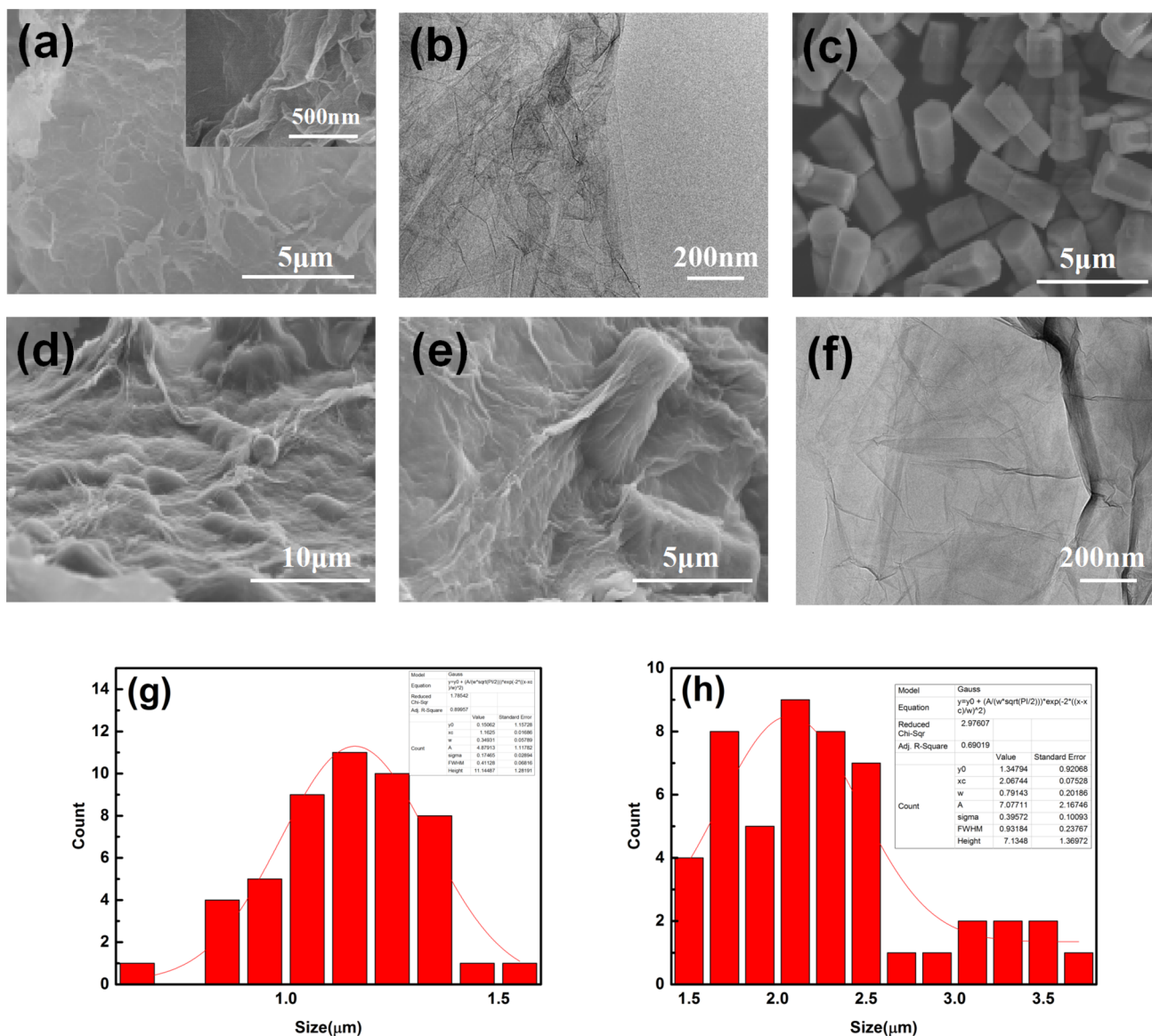
Fig. 2 SEM (**a**) and TEM (**b**) images of RGO, (**c**) SEM image of ZnO-mrs, SEM (**d**, **e**) and TEM (**f**) images of RGO/ZnO-mrs-2; the length statistics (**g**) and short diameter statistics (**h**) of ZnO-mrs

to electromagnetic wave. According to the data in Fig. 4a and b, $\tan\delta_E$ values of materials are calculated and shown in Fig. 4e. In range of 2–15 GHz, $\tan\delta_E$ values of RGO are the highest, suggesting their strongest dielectric loss to EMW. The $\tan\delta_E$ values of composites decrease with the addition of ZnO-mrs, and for pure ZnO-mrs has almost no dielectric loss. But when f exceeds 15 GHz, the $\tan\delta_E$ value of RGO/ZnO-mrs-1 exceeds that of RGO, which may be attributed to the addition of ZnO-mrs, the dielectric loss ability to EMW of RGO/ZnO-mrs-1 is better than that of RGO, meanwhile the interface polarization loss and dipole polarization loss of RGO/ZnO-mrs-1 are stronger than those of RGO. It should be noted that the vibration peaks

caused by relaxation behavior can be viewed at about 16.4, 15.9, 14.3 and 11.6 GHz for RGO, RGO/ZnO-mrs-1, RGO/ZnO-mrs-2 and RGO/ZnO-mrs-3, respectively. In general, relaxation usually occurs when the orientation velocity of dipole pairs cannot keep pace with the changes of the external electric field. The dipole polarization is caused by the defects and the polar oxygen-containing functional groups in RGO [30]. It can be seen that the relaxation frequency moves to low frequency with the increase of ZnO-mrs load. This work, in alternating electromagnetic field, a large number of dipole pairs may accumulate on the surfaces of GO sheets and change their direction with the incident electromagnetic wave. However, with the addition of ZnO-mrs, which could
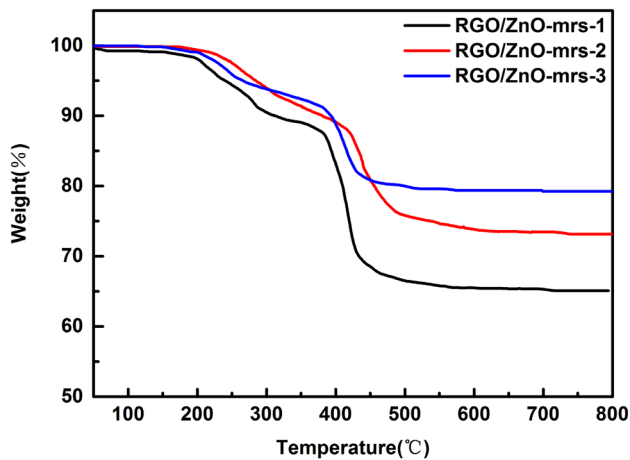
Fig. 3 TG curves of RGO/ZnO-mrs

hinder the movement of dipole pairs, the larger the load of ZnO-mrs is, the more obvious the blocking effect is, and the lower the relaxation frequency is. When no interaction exists, the relaxation frequency would be determined only by the inherent characteristics of the material [31].

As is known to all, Debye relaxation is an important mechanism of dielectric loss materials. According to Debye theory, the dielectric properties of materials can be explained based on Cole–Cole model [32], because the relations between ε' and ε'' can be expressed as by Formula 1

$$\left(\varepsilon' - \frac{\varepsilon_s - \varepsilon_\infty}{2}\right)^2 + (\varepsilon'')^2 = \left(\frac{\varepsilon_s - \varepsilon_\infty}{2}\right)^2 \qquad (1)$$

Figure 5 shows the Cole–Cole curves of RGO and RGO/ZnO-mrs in range of 2.0–18.0 GHz. As shown in Fig. 5a, an irregular semicircle and a long tail can be observed, which ascribes there is a strong conduction loss and a weak polarization loss process in RGO. In Fig. 5b, it is observed that the tail becomes shorter and the semicircle becomes regular with the addition of ZnO-mrs, suggesting that the polarization loss gets stronger, but the conduction loss is still the dominant process. In Fig. 5c, there are two semicircles and a small tail in curve of RGO/ZnO-mrs, indicating that there are two kinds of polarization processes and the polarization loss dominates accompanied by the conduction loss [31]. In Fig. 5d, there are several irregular semicircles in ε'–ε'' curve of RGO/ZnO-mrs with a small tail, it can be explained that the polarization loss and conductivity loss are all relatively weak, which is not conducive to microwave absorption performance

To evaluate and compare the effects of the amounts of ZnO-mrs added on the microwave absorbing properties

of composites prepared, based on the transmission line theory, their RL values were calculated by the following equations [33]:

$$RL(dB) = 20 \log |(Z_{in} - Z_0)/(Z_{in} + Z_0)| \qquad (2)$$

$$Z_{in} = Z_0(\mu_r/\varepsilon_r)1/2 \tanh[(j2\pi fd/c)(\mu_r\varepsilon_r)^{1/2}] \qquad (3)$$

where Z_0 is the characteristic impedance of free space (377 Ω), Z_{in} is the input impedance, f is the frequency of electromagnetic wave, c is the speed of electromagnetic wave in free space, d is thickness of microwave absorbing materials, and ε_r and μ_r are their complex permittivity and complex permeability, respectively.

When reflection loss (RL) of material is less than − 10 dB, it means that this material can effectively absorb more than 90% of EMW, which can meet the requirements of practical microwave absorption applications, and the corresponding frequency range can be considered as the EAB. Figure 6 shows RL–f curves calculated in range of 2–18 GHz of materials with different thicknesses. It can be seen that the microwave absorption performance of RGO is poor, while ZnO-mrs has almost no microwave absorption performance, showing that the single conductive material or semiconductor material cannot possess a good microwave absorption performance. As shown in Fig. 6c, when the thickness of RGO/ZnO-mrs-1 is 2.5 mm, its RL_{min} only reaches − 13.9 dB at 10 GHz and EAB is only 2.8 GHz (8.9–11.7 GHz). The absorption properties of RGO/ZnO-mrs-3 are similar to those of RGO/ZnO-mrs-1, when the thickness is 3 mm, its RL_{min} only reaches − 11.9 dB at 10 GHz and EAB is only 1.5 GHz (10.9–12.4 GHz). RGO/ZnO-mrs-2 shows the best microwave absorption performance, its RL_{min} is − 38.5 dB and EAB is 5.4 GHz (12.6–18 GHz) with thickness of 2 mm only.

It also can be seen that the load of ZnO-mrs has a great influence on EMW absorption properties of composites. When the load of ZnO-mrs in composite is less, its dielectric constant and conductivity are relatively higher, leading to the weaker EMW absorption. With the increase of ZnO-mrs load, conductivity of composites slightly decreases, and its dielectric constant decreases too. However, increase of the interfaces of composites, such as RGO/ZnO-mrs-2, leads to the interface polarization between RGO and ZnO-mrs playing a key role in its polarization loss. Therefore, RGO/ZnO-mrs-2 has an outstanding absorption performance. So it can be inferred that the interface polarization can effectively enhance the dielectric loss capacity of material when the increase of its conductivity is limited. According to the above analyses of Cole–Cole, it can be seen that RGO/ZnO-mrs-3 has poor EMW absorption performance, which is attributed to the low dielectric loss. It can be observed that RL_{min} of all
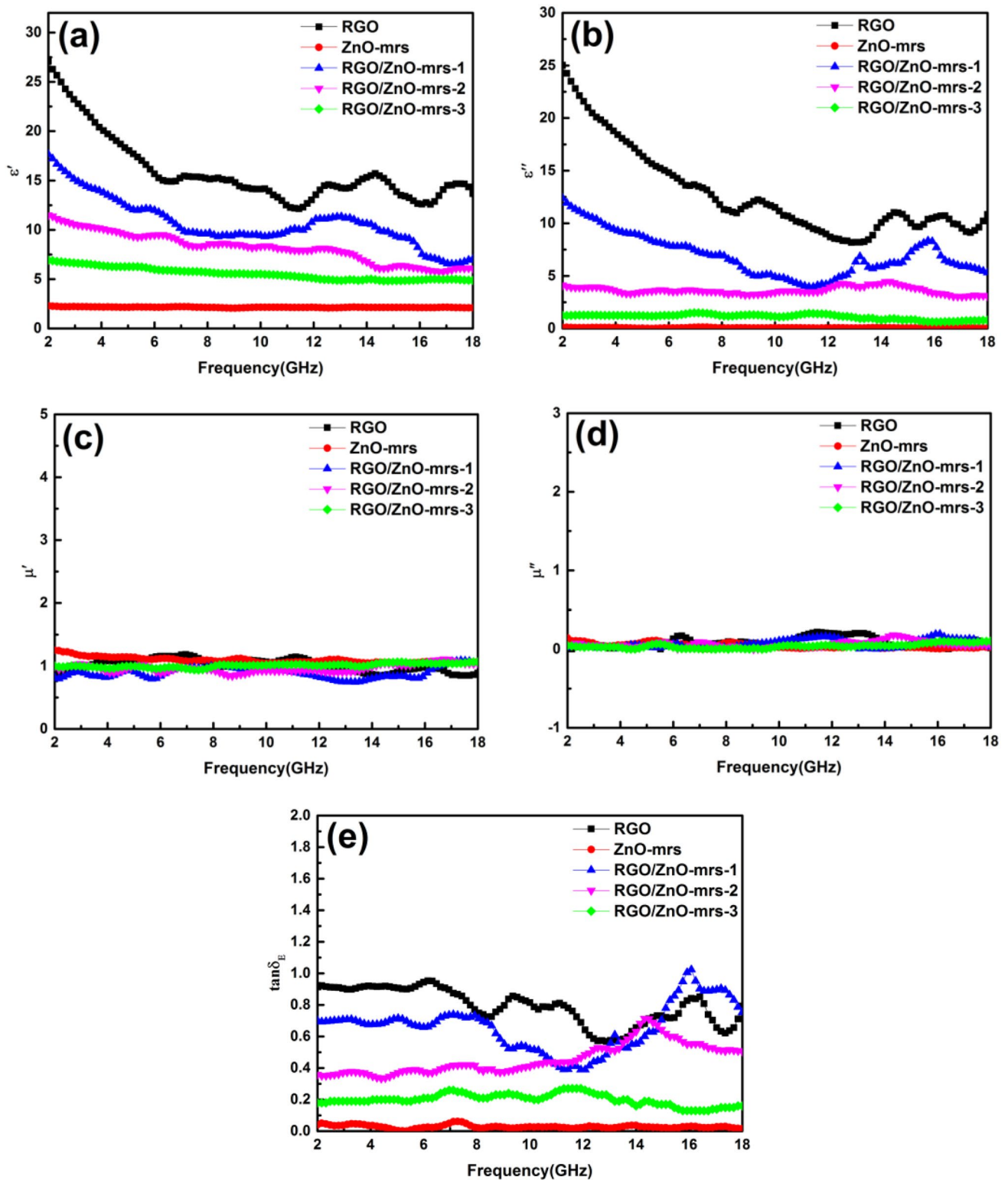
Fig. 4 Frequency dependence of (**a**) real and (**b**) imaginary parts of permittivity and (**c**) real and (**d**) imaginary parts of permeability and (**e**) the dielectric loss tangents of RGO, ZnO-mrs and RGO/ZnO-mrs

materials moves to the low frequency with the increase of their thickness, which is due to the quarter wavelength

interference cancellation principle, that is, when thickness of the composite is an odd multiple of quarter wavelength,
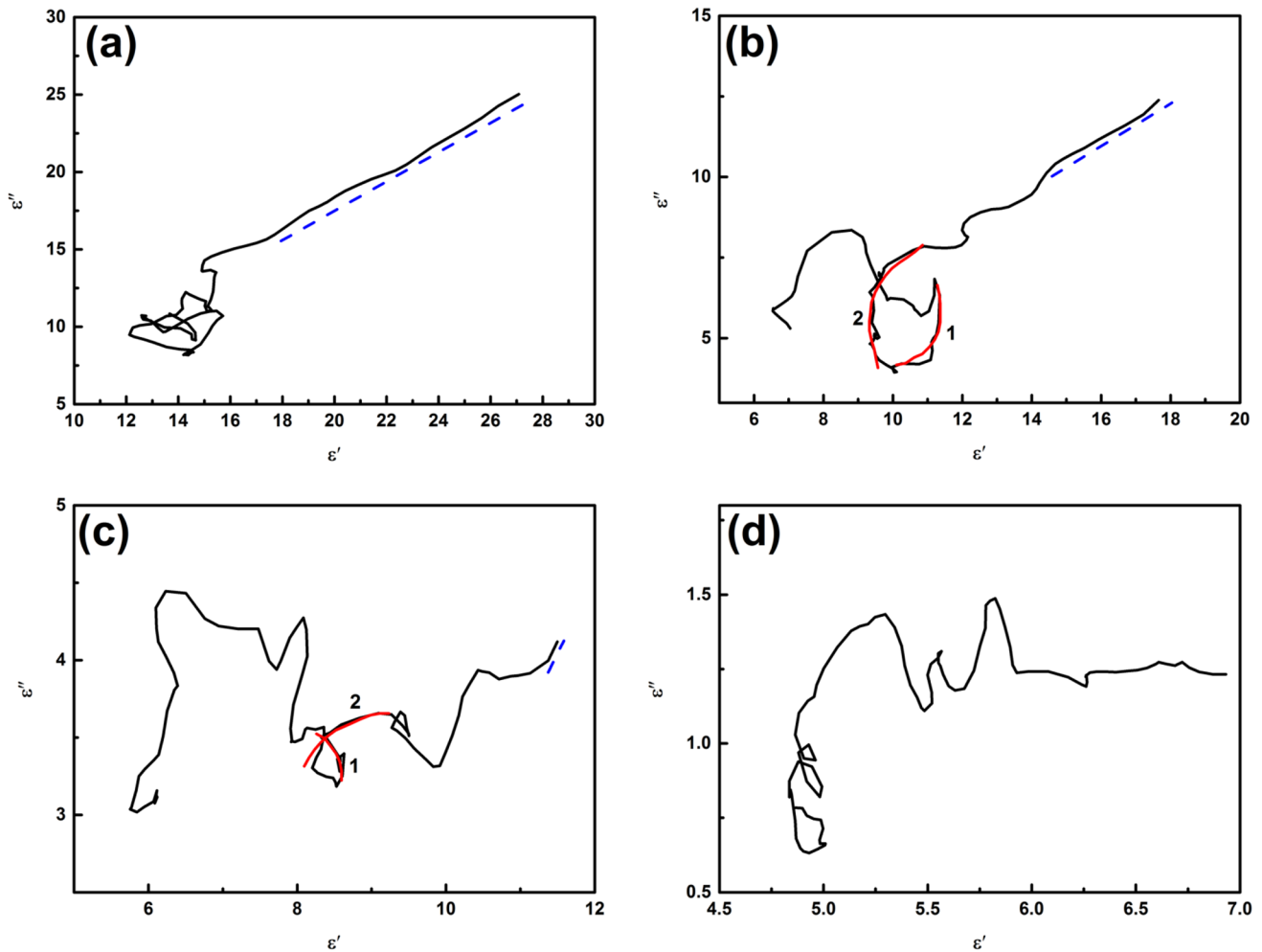
Fig. 5 ε'–ε'' curves of (**a**) RGO, (**b**) RGO/ZnO-mrs-1, (**c**) RGO/ZnO-mrs-2 and (**d**) RGO/ZnO-mrs-3

the two EMW reflected from the upper and lower interfaces of this material will cancel each other at a certain frequency, corresponding to RL_{min} [14]. In addition to the loss capacity, impedance matching with free space is another important factor affecting the microwave absorption properties of the material. Equations of impedance matching and attenuation constant are as follows [34].

$$Z = |Z_{in}/Z_0| = (\mu_r/\varepsilon_r)1/2 \tanh[(j2\pi fd/c)(\mu_r\varepsilon_r)^{1/2}] \quad (4)$$

$$\alpha = \frac{\sqrt{2\pi f}}{c} \times \sqrt{(\mu'\varepsilon'' - \mu'\varepsilon') + \sqrt{(\mu'\varepsilon'' - \mu'\varepsilon')^2 + (\varepsilon'\mu'' + \varepsilon''\mu')^2}} \quad (5)$$

When the value of Z is close to 1, the perfect impedance matching between material and free space can be achieved, that is, the EMW is not reflected by surface of the material and all enters inside the material; when the value of Z is far away from 1, only limited impedance matching between material and free space can be achieved.

When $0.52 < Z < 1.96$, effective absorption ($RL < -10$ dB) can be achieved, which may be named effective impedance matching between material and free space [35, 36]. Figure 7a shows the Z–f curves of the related composites with RL_{min}. It can be seen that Z value of RGO is less than 0.52 in range of 2–18 GHz, indicating that RGO has not achieved effective impedance matching with free space in the whole frequency band. After the introduction of ZnO-mrs, the impedance matching performance with free space of the composites is significantly improved, because the conductivity and permittivity of materials are all decreased, making their Z values reach an effective range. As can be seen that RGO/ZnO-mrs-2 has better impedance matching with free space than the other composites, which can make more EMW enter inside this composite; especially, it has effective impedance matching with free space in the frequency range of 9–18 GHz. The attenuation constant represents the loss capacity to EMW of materials, and Fig. 7b shows curves of the attenuation
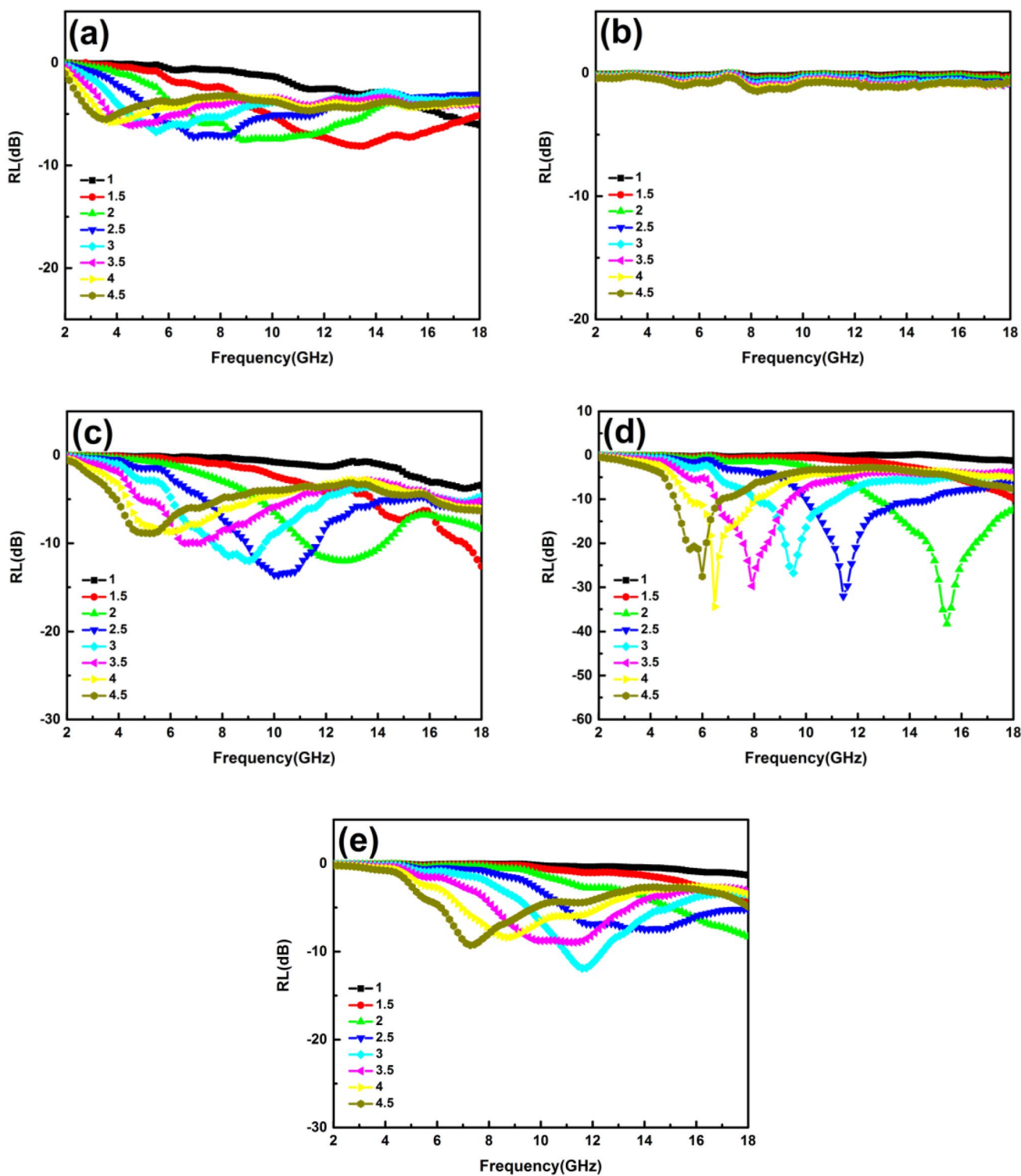
Fig. 6 RL-*f* curves of (**a**) RGO, (**b**) ZnO-mrs, (**c**) RGO/ZnO-mrs-1, (**d**) RGO/ZnO-mrs-2 and (**e**) RGO/ZnO-mrs-3 with different thickness

constant of composites to EMW changing with frequency. It can be seen that the attenuation ability to EMW of RGO is the strongest, and the attenuation constant to EMW of RGO/ZnO-mrs decreases with the increase of ZnO-mrs

load, suggesting that material must have excellent impedance matching with free space and attenuation ability to EMW at the same time to obtain good EMW absorption performance.
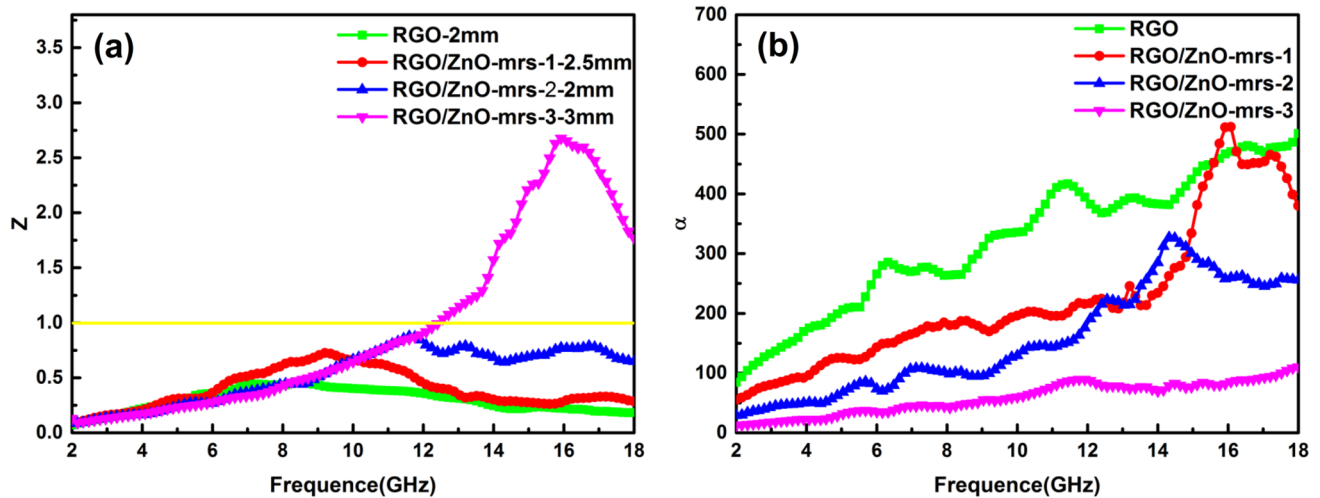
Fig. 7 (a) Z–f curves of composites with RL_{min} at corresponding thickness. (b) α–f curves of RGO and RGO/ZnO-mrs

Table 1 Typical RGO/ZnO composites for electromagnetic microwave absorption

Absorber	Matrix	Absorber content (wt%)	RL_{min} (dB)	Optimum thickness (mm)	EAB (RL < − 10 dB)	References
Starlike ZnO/RGO doped by nanocrystals/RGO	Paraffin	25	− 77.5	4.5	6.9	[19]
RGO/ZnO/Fe$_3$O$_4$	Paraffin	15	− 35.0	5.0	5.4	[14]
RGO/ZnO hollow spheres	Paraffin	50	− 45.0	2.2	3.3	[27]
3Dgraphene/shuttle-shaped ZnO	Paraffin	25	− 23.3	1.5	4.1	[20]

With the comparisons of EMW absorption performances of typical RGO/ZnO-based composites reported recently and in our research, Table 1 shows their microwave absorption properties. Compared with other studies reported, RGO/ZnO-mrs composite prepared by this research possesses an outstanding comprehensive performance, that is, wide EAB and low loading concentration, especially with the simple and expandable preparing process, demonstrating a promising prospect in the development of light weight and excellent microwave absorption applications.

From above analyses, it can be seen that the outstanding EMW absorption properties of composite RGO/ZnO-mrs can be attributed to the reasons as follows. First, ZnO-mrs can prevent effectively the agglomeration of RGO sheets, and the conductivity between RGO and ZnO-mrs is very different, not only will there be many dipole pairs at the interface between RGO and ZnO-mrs, but also the interfaces between ZnO-mrs and RGO increase greatly with the increase of ZnO-mrs load in composite, which leads to the interfacial polarization generally occurring in heterostructure (namely Maxwell Wagner effect); more importantly, interfacial area is the most important factor in regulating interface polarization [37, 38]. Second, defects and residual oxygen-containing functional groups in RGO can serve as polarized centers, leading to strong electromagnetic wave absorption [30]. Furthermore, the dipole pairs in these defects caused by chemical reduction cannot respond to the applied high-frequency alternating electromagnetic field as soon as possible, which results in dipole orientation polarization and dipole polarization relaxation processes with strong EMW attenuation. In addition, conduction loss should also be emphasized, RGO sheets can provide free electrons and ZnO-mrs can be regarded as the resistance, electrons would be driven in the opposite direction with external field of the external electromagnetic field, resulting in induced current, and based on Ohm's law, energy will be consumed in the form of Joule heat [31]. Finally, impedance matching between free space and composite is effectively improved by controlling the load of ZnO-mrs, thereby reducing the reflection to EMW on the material surface, so the balance between attenuation ability to EMW and impedance matching between composite and free space is achieved.

4 Conclusions

Outstanding EMW absorbing composite, RGO decorated with ZnO-mrs, was produced by a simple mechanical mixing and direct freeze-drying method, and its structure, morphology and component ratio were characterized by XRD, Raman, SEM, XPS and TG methods. Both excellent impedance matching with the free space and strong loss capacity to EMW, including conduction loss, interfacial polarization and dipole polarization, of RGO/ZnO-mrs can all be controlled effectively by adjusting the load of ZnO-mrs in composite. When mass ratio of RGO and ZnO is 1:3, composite RGO/ZnO-mrs shows the most excellent EMW absorption properties, RL_{min} of -38.5 dB at 15.4 GHz and EAB reaches 5.4 GHz (12.6–18 GHz) with thickness of 2 mm and filling rate of 15 wt% only. Therefore, it is believed that composite RGO/ZnO-mrs would be widely used in the field of EME absorption due to its high-performance absorption, low filling concentration, especially the simple and expandable preparing process.

References

1. L. Yan, C. Hong, B. Sun, G. Zhao, Y. Cheng, S. Dong, D. Zhang, X. Zhang, In situ growth of core-sheath heterostructural SiC nanowire arrays on carbon fibers and enhanced electromagnetic wave absorption performance. Acs. Appl. Mater. Interfaces **7**, 6320–6331 (2017)
2. P. Liu, Y. Huang, J. Yan, Y. Yang, Y. Zhao, Construction of CuS nanoflakes vertically aligned on magnetically decorated graphene and their enhanced microwave absorption properties. Acs. Appl. Mater. Interfaces **8**, 5536–5546 (2016)
3. Y. Nariman, S. Xinying, L. Xiuyi, S. Xi, J. Jingjing, Z. Biao, T. Benzhong, C. Mansun, K. Jang-Kyo, Highly aligned graphene/polymer nanocomposites with excellent dielectric properties for high-performance electromagnetic interference shielding. Adv. Mater. **26**, 5480–5487 (2014)
4. K. Luo, X. Yin, Y. Zhang, X. Yuan, L. Zhang, Electromagnetic wave absorption properties of reduced graphene oxide modified by maghemite colloidal nanoparticle glusters. J. Phys. Chem. C **117**, 19701–19711 (2013)
5. P. Liu, Y. Jing, X. Gao, H. Ying, Y. Zhang, Construction of layer-by-layer sandwiched graphene/polyaniline nanorods/carbon nanotubes heterostructures for high performance supercapacitors. Electrochim. Acta **272**, 77–87 (2018)
6. H. Chen, Z. Huang, Y. Huang, Y. Zhang, Z. Ge, B. Qin, Z. Liu, Q. Shi, P. Xiao, Y. Yang, T. Zhang, Y. Chen, Synergistically assembled MWCNT/graphene foam with highly efficient microwave absorption in both C and X bands. Carbon. **124**, 506–514 (2017)
7. Y. Zhang, Y. Huang, H. Chen, Z. Huang, Y. Yang, P. Xiao, Y. Zhou, Y. Chen, Composition and structure control of ultralight graphene foam for high-performance microwave absorption. Carbon. **105**, 438–447 (2016)
8. A. Abouimrane, O.C. Compton, K. Amine, S.B.T. Nguyen, Non-annealed graphene paper as a binder-free anode for lithium-ion batteries. J. Phys. Chem. C **29**, 12800–12804 (2010)
9. C.N.R. Rao, A.K. Sood, K.S. Subrahmanyam, A. Govindaraj, Graphene: The new two-dimensional nanomaterial. Chem. Int. Edit. **48**, 7752–7777 (2009)
10. Z. Yi, H. Yi, Z. Tengfei, C. Huicong, X. Peishuang, C. Honghui, H. Zhiyu, C. Yongsheng, Broadband and tunable high-performance microwave absorption of an ultralight and highly compressible graphene foam. Adv. Mater. **12**, 2049–2053 (2015)
11. L. Zhu, X. Zeng, X. Li, B. Yang, R. Yu, Hydrothermal synthesis of magnetic Fe_3O_4/graphene composites with good electromagnetic microwave absorbing performances. J. Magn. Magn. Mater. **426**, 114–120 (2017)
12. Y.F. Bai, W.H. Ma, Y.A. Liu, Y. Liu, J.W. Xue, K. Xu, Y.Q. Liu, G.Z. Zhao, Preparation of graphene-carbonyl iron powder@tri-iron tetroxide composite and its better microwave absorption properties. J. Mater. Sci-Mater. El. **30**, 5454–5463 (2019)
13. X.Y. Liu, Y.Q. Gao, G.W. Yang, A flexible, transparent and super-long-life supercapacitor based on ultrafine Co_3O_4 nanocrystal electrodes. Nanoscale. **7**, 4227–4235 (2016)
14. N. Zhang, Y. Huang, M. Wang, 3D ferromagnetic graphene nanocomposites with ZnO nanorods and Fe_3O_4 nanoparticles co-decorated for efficient electromagnetic wave absorption. Composites B **136**, 135–142 (2018)
15. K. Xu, W. Ma, Y. Liu, Y. Bai, J. Xue, Y. Liu, G. Zhao, Y. Liu, Broadband and tunable highperformance microwave absorption composites reduced graphene oxide Ni. J. Mater. Sci-Mater. El. **30**, 1–10 (2019)
16. Y.L. Jing, J. Guo Wen, F.R. Zhi, Hierarchical ZnO nanostructures. Nano Lett. **11**, 1287–1291 (2002)
17. Ü Özgür, Y.I. Alivov, C. Liu, A. Teke, M.A. Reshchikov, S. Doğan, V. Avrutin, S.J. Cho, H. Morkoç, A comprehensive review of ZnO materials and devices. J. Appl. Phys. **4**, 11–11 (2005)
18. C. Song, X. Yin, M. Han, X. Li, Z. Hou, L. Zhang, L. Cheng, Three-dimensional reduced graphene oxide foam modified with ZnO nanowires for enhanced microwave absorption properties. Carbon. **116**, 50–58 (2017)
19. W. Feng, Y. Wang, J. Chen, L. Guo, J. Ouyang, D. Jia, Y. Zhou, Microwave absorbing property optimization of starlike ZnO/reduced graphene oxide doped by ZnO nanocrystal composites. Phys. Chem. Chem. Phys. **19**, 14596–14605 (2017)
20. S. Yang, X. Guo, P. Chen, D.W. Xu, H.F. Qiu, X.Y. Zhu, Two-step synthesis of self-assembled 3D graphene/shuttle-shaped zinc oxide (ZnO) nanocomposites for high-performance microwave absorption. J. Alloys Compd. **797**, 1310–1319 (2019)
21. L. Tang, W. Ying, Y. Li, H. Feng, J. Li, Preparation, structure, and electrochemical properties of reduced graphene sheet films. Adv. Funct. Mater. **17**, 2782–2789 (2009)
22. D. Qi, L. Zheng, X. Cao, Y. Jiang, H. Xu, Y. Zhang, B. Yang, Y. Sun, H.H. Hng, N. Lu, Bio-inspired antireflective hetero-nanojunctions with enhanced photoactivity. Nanoscale. **5**, 12383–12387 (2013)
23. Z. Yanwu, M. Shanthi, C. Weiwei, L. Xuesong, S.J. Won, J.R. Potts, R.S. Ruoff, Graphene and graphene oxide: synthesis, properties, and applications. Adv. Mater. **35**, 3906–3924 (2010)
24. N.J. Bell, H.N. Yun, A. Du, H. Coster, S.C. Smith, R. Amal, Understanding the enhancement in photoelectrochemical properties of photocatalytically prepared TiO_2-reduced graphene oxide composite. J. Phy. Chem. C **13**, 6004–6009 (2011)
25. S. Pei, C.H.E.N.G. HuiMing, The reduction of graphene oxide. Carbon. **9**, 3210–3228 (2012)
26. Z. Yi, H. Yi, H. Chen, Z. Huang, Y. Yang, P. Xiao, Z. Ying, Y. Chen, Composition and structure control of ultralight graphene

foam for high-performance microwave absorption. Carbon. **105**, 438–447 (2016)

27. M. Han, X. Yin, L. Kong, M. Li, W. Duan, L. Zhang, L. Cheng, Graphene-wrapped ZnO hollow spheres with enhanced electromagnetic wave absorption properties. J. Mater. Chem. A. **39**, 16403–16409 (2014)

28. X. Jian, B. Wu, Y. Wei, S. Dou, X. Wang, W. He, N. Mahmood, Facile synthesis of Fe_3O_4/GCs composites and their enhanced microwave absorption properties. Acs. Appl. Mater. Interfaces **8**, 6101 (2016)

29. W.L. Song, M.S. Cao, B. Wen, Z.L. Hou, J. Cheng, J. Yuan, Synthesis of zinc oxide particles coated multiwalled carbon nanotubes: dielectric properties, electromagnetic interference shielding and microwave absorption. Mater. Res. Bull. **7**, 1747–1754 (2012)

30. Y. Chen, A. Zhang, L. Ding, Y. Liu, H. Lu, A three-dimensional absorber hybrid with polar oxygen functional groups of MWNTs/graphene with enhanced microwave absorbing properties. Composites B **108**, 386–392 (2017)

31. W. Liu, S. Tan, Z. Yang, G. Ji, Hollow graphite spheres embedded in porous amorphous carbon matrices as lightweight and low-frequency microwave absorbing material through modulating dielectric loss. Carbon. **138**, 143–153 (2018)

32. J. Zou, Z. Wang, M. Yan, H. Bi, Enhanced interfacial polarization relaxation effect on microwave absorption properties of submicron-sized hollow Fe_3O_4 hemispheres. J. Phys. D Appl. Phys. **47**, 275001 (2014)

33. X. Bai, Y. Zhai, Y. Zhang, Green approach to prepare graphene-based composites with high microwave absorption capacity. J. Phys. Chem. C **115**, 11673–11677 (2011)

34. J. Fang, T. Liu, Z. Chen, Y. Wang, W. Wei, X. Yue, Z. Jiang, A wormhole-like porous carbon/magnetic particles composite as an efficient broadband electromagnetic wave absorber. Nanoscale. **16**, 8899–8909 (2016)

35. S. Dai, B. Quan, B. Zhang, X. Liang, G. Ji, Constructing multi-interface Mo_2C/Co@C nanorods for a microwave response based on a double attenuation mechanism. Dalton. Trans. **41**, 14767–14773 (2018)

36. W. Liu, L. Liu, Z. Yang, J. Xu, Y. Hou, G. Ji, A versatile route toward the electromagnetic functionalization of metal-organic framework-derived three-dimensional nanoporous carbon composites. Acs. Appl. Mater. Interface **10**, 8965–8975 (2018)

37. Z. Wang, L. Wu, J. Zhou, Z. Jiang, B. Shen, Chemoselectivity-induced multiple interfaces in MWCNT/Fe_3O_4@ZnO heterotrimers for whole X-band microwave absorption. Nanoscale **21**, 12298–12302 (2014)

38. K. Luo, X. Yin, Y. Zhang, X. Yuan, L. Quan, Y. Fang, L. Cheng, L. Zhang, Electromagnetic wave absorption properties of reduced graphene oxide modified by maghemite colloidal nanoparticle clusters. J. Phys. Chem. C **117**, 19701–19711 (2013)